The Astrophysical Journal, 656:914–927, 2007 February 20

THE FRAGMENTING SUPERBUBBLE ASSOCIATED WITH THE H II REGION W4

Jennifer L. West and Jayanne English
Department of Physics and Astronomy, University of Manitoba, Winnipeg, MB, Canada;
jennifer_west@umanitoba.ca, english@physics.umanitoba.ca

Magdalen Normandeau[1]
Department of Physics, Amherst College, Amherst, MA; mnormandeau@amherst.edu

and

T. L. Landecker
Dominion Radio Astrophysical Observatory, Herzberg Institute of Astrophysics, National Research Council,
Penticton, BC, Canada; tom.landecker@nrc.gc.ca
Received 2005 June 23; accepted 2006 November 3

ABSTRACT

New observations at high latitudes above the H II region W4 show that the structure formerly identified as a chimney candidate, an opening to the Galactic halo, is instead a superbubble in the process of fragmenting and possibly evolving into a chimney. Data at high Galactic latitudes ($b > 5^\circ$) above the W3/W4 star-forming region at 1420 and 408 MHz Stokes I (total power) and 1420 MHz Stokes Q and U (linear polarization) reveal an egg-shaped structure with morphological correlations between our data and the Hα data of Dennison, Topasna, and Simonetti. Polarized intensity images show depolarization extending from W4 up the walls of the superbubble, providing strong evidence that the radio continuum is generated by thermal emission coincident with the Hα emission regions. We conclude that the parts of the H II region hitherto known as W4 and the newly revealed thermal emission are all ionized by the open cluster OCl 352. At an assumed distance of 2.35 kpc, the ovoid structure is 164 pc wide and extends 246 pc above the midplane of the Galaxy. The shell's emission decreases in total intensity and polarized intensity in various locations, appearing to have a break at its top and another on one side. Using a geometric analysis of the depolarization in the shell's walls, we estimate that a magnetic field line-of-sight component of 3–5 μG exists in the shell. We explore the connection between W4 and the Galactic halo, considering whether sufficient radiation can escape from the fragmenting superbubble to ionize the kiloparsec-scale Hα loop discovered by Reynolds, Sterling and Haffner.

Subject headings: ISM: bubbles — ISM: kinematics and dynamics — stars: winds, outflows

1. INTRODUCTION

Theory suggests that supernovae and/or winds from massive stars existing in clusters confined to the disk of the Galaxy produce bubbles in the interstellar medium (ISM) that expand, becoming superbubbles, and burst out of the Galactic disk producing collimated outflows into the Galactic halo (Norman & Ikeuchi 1989; Tenorio-Tagle & Bodenheimer 1988). The superbubbles, which create cavities in the atomic hydrogen gas in the disk of the Galaxy, contain a plasma of hot gas, high-energy photons, and cosmic rays (CRs). When a bubble's wall bursts at high latitudes the structure is termed a "chimney," since the cavity and its walls act as a conduit for the outflow of this plasma toward the halo of the Galaxy (see, e.g., de Avillez & Berry 2001). In addition, the magnetic field that is oriented parallel to the disk of the Galaxy is frozen into the plasma and is thus pulled upward with the shell material as the bubble expands. Consequently, it is predicted that these conduits should have magnetic field lines that run tangential to the shell (Norman & Ikeuchi 1989; Basu et al. 1999, hereafter BJM99).

An unusual, cone-shaped void observed in neutral hydrogen (Normandeau et al. 1996, hereafter NTD96), which has the star cluster OCl 352 at its base, is one of the few observationally identified Galactic chimney candidates and has come to be known as the "W4 chimney." It was proposed that the region has been evacuated of H I by the winds of nine O-type stars that are part of the open cluster OCl 352. In this case the stellar wind scenario is favored over the supernovae scenario, since the cluster seems too young to have had any supernovae occur and the energy output of the winds appears to be sufficient to account for the void (NTD96). Estimates of the age of OCl 352 range from 1.3–2.5 Myr (Dennison et al. 1997, hereafter DTS97, and references therein) to 3.7–4.3 Myr (NTD96). We adopt a distance to the region of 2.35 kpc.

The "chimney" region is located above OCl 352 and is a distinct component from the ionized "W4 loop," which is located below OCl 352 (Normandeau et al. 1997). We consider only the structure that is above the star cluster and above the ridge of ionized gas that defines the upper latitude structure of the W4 H II region. The H I images (see NTD96 and Figs. 1 and 2) make it clear that the regions above and below the cluster, i.e., above and below the upper ionized ridge of W4, are different in nature: the upper region has been mostly cleared of H I, hence the possibility that it is a chimney or a superbubble. The lower region has not been cleared, at least not at the same velocities.

The interpretation of Terebey et al. (2003) and BJM99 that the superbubble structure includes the W4 loop is in contrast to this picture. While it is likely that both the W4 loop and the structure above W4 are powered by the same stars, they do not form one

[1] Current address: Department of Physics, University of New Brunswick, Fredericton, NB, Canada.

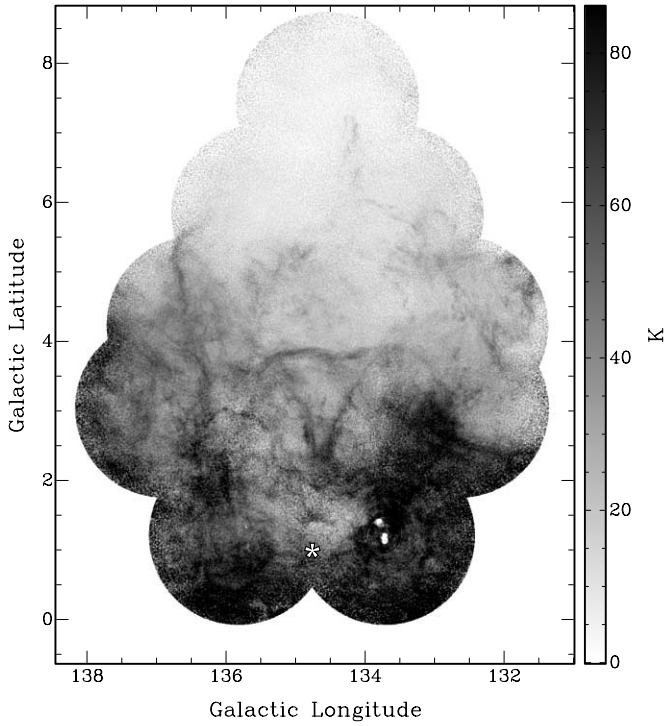

FIG. 1.—G134.4+3.85 in H I centered at −43.40 km s^{-1} with a channel width of 2.64 km s^{-1}. The asterisk marks the approximate location of OCl 352.

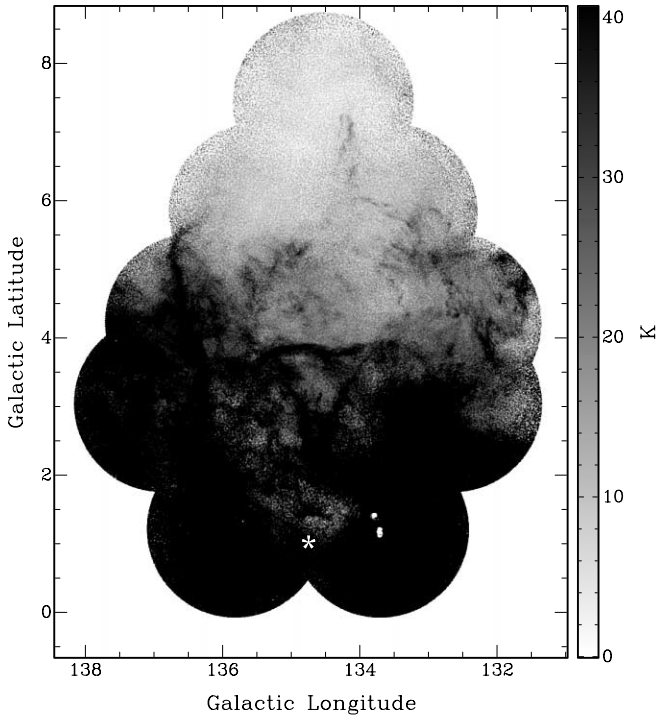

FIG. 2.—Same as Fig. 1, but with a gray scale chosen to highlight the faint upper latitude structures.

dynamical entity. The use of the term "chimney" provides a metaphor only for the part of the structure above W4, since a chimney not only has walls but also has a fire at its base. In this case the fire is the OCl 352 cluster. To avoid unwieldy nomenclature, rather than referring to the structure as the "W4 superbubble/chimney," we dub it G134.4+3.85. The new name, however, should not be understood as implying that G134.4+3.85 has a different origin from W4. Indeed we argue that both objects are thermal emission regions excited by the open cluster OCl 352.

In the radio regime, at Galactic latitudes of less than +4°, the structure is reminiscent of the conventional chimney model of Norman & Ikeuchi (1989), i.e., a broken H I shell allowing CRs and UV photons to escape to higher latitudes. The contrasting analysis of DTS97, using narrowband Hα data, is that W4 is an "apparently closed superbubble." However, the DTS97 data suffer from substantial vignetting at the field edges, which could lead the eye to see a bubble shape where none exists. This makes corroboration from other data sets desirable. In addition, the DTS97 data do not include velocity information, which means that the observed Hα emission could be from unrelated sources along the line of sight.

BJM99 considered both the dynamics (Kompaneets modeling) and the ionization of the superbubble based on the Hα data from DTS97. Of particular interest here is the conclusion of BJM99 that an open geometry in H I images and a closed one in data showing ionized gas are not mutually exclusive. The superbubble's shell could be sufficiently thin at high latitudes that while it closes the shell and prevents streaming of gas toward higher latitudes, it does not hold back the ionizing radiation that then obliterates the H I at higher latitudes. This scenario is in fact likely according to these authors.

In this paper we present new observations of radio continuum and H I emission, extending coverage from $b = 5°$, the limits of earlier data, to $b = 8.5°$. We analyze the H I spectral line emission as well as the 1420 and 408 MHz radio continuum emission from this region for evidence supporting either the chimney or the superbubble picture. For the 1420 MHz continuum data, full polarization information is available. The data acquisition and processing are described in § 2. Image mosaics and false-color morphological analysis are presented in § 3.1. The H I emission is addressed in § 3.2. The polarization data are discussed in § 3.3. The interrelationship between emission components is discussed in § 4, and the magnetic field of the region is explored, using our polarization data, in § 5.

Our analysis creates a picture of a *fragmented* superbubble above W4, G134.4+3.85, which may be in the process of evolving into a chimney, possibly due to magnetic effects. While we use two separate names, we believe that both "objects" are the outcome of the ionizing flux from OCl 352 and are therefore in some sense just one object. In § 6 we discuss this picture, superbubble formation scenarios, and the superbubble's connection to the Galactic halo. The paper is summarized in § 7.

2. DATA

2.1. *Acquisition*

Landecker et al. (2000) provide a complete description of the Dominion Radio Astrophysical Observatory (DRAO) Synthesis Telescope. The Synthesis Telescope is an east-west array of seven antennas with diameters ∼9 m. Of these seven, four are fixed and three are movable, allowing sampling of baselines from 12.86 to 604.29 m in steps of 4.29 m. At $\lambda = 21$ cm, this corresponds to coverage on all spatial scales from ∼1′ to 56′. The data collected consist of several components: spectral line emission from atomic hydrogen at $\lambda = 21.1$ cm, continuum emission at 1420 MHz with full polarization information, and continuum emission at 408 MHz.

The DRAO Synthesis Telescope recently completed Phase I of the Canadian Galactic Plane Survey (CGPS; Taylor et al. 2003). The CGPS is a relatively high resolution (∼1′ at 1420 MHz; ∼3.7′ at 408 MHz) data set covering 73.1° in longitude, from $\ell = 74.2°$ to 147.3° along the Galactic plane of the Milky Way. The latitude extent covers $-3.6° < b < +5.6°$. Three higher latitude

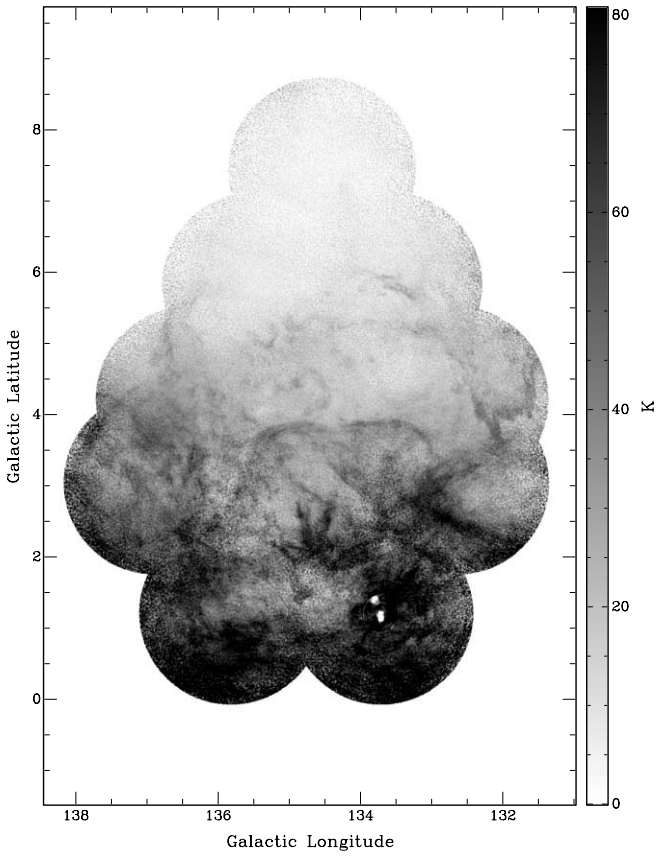

FIG. 3.—G134.4+3.85 in H I centered at -40.11 km s^{-1} with a channel width of 2.64 km s^{-1}. This channel represents the upper limit at which the structure of G134.4+3.85 can still be easily identified.

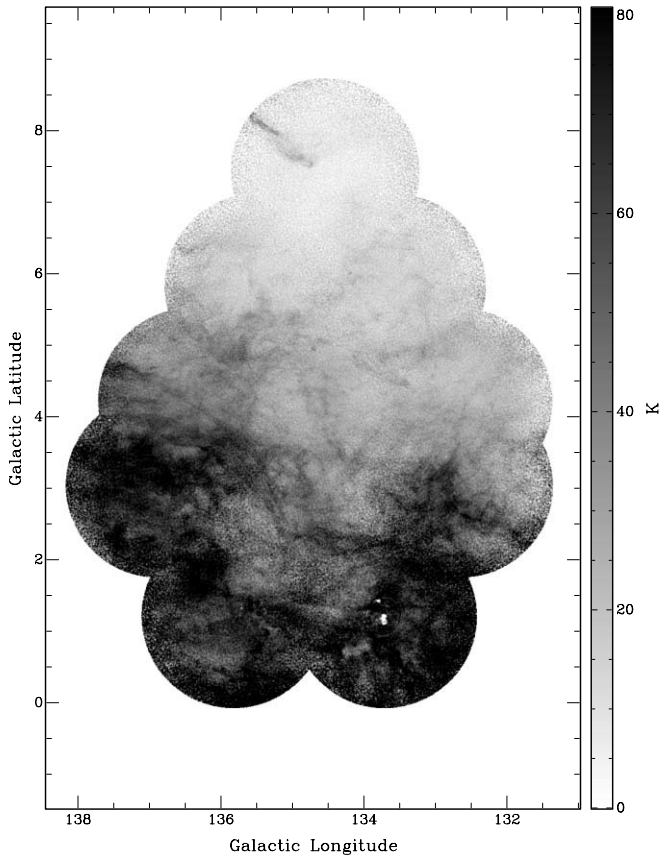

FIG. 4.—Same as Fig. 3, but centered at -48.35 km s^{-1}. This channel represents the lower limit at which the structure of G134.4+3.85 can still be easily identified.

fields, on an extension of the CGPS grid, were acquired for the present study.

At 1420 MHz the field of view of the Synthesis Telescope has a full width at half-maximum (FWHM) of 107.2′. At 408 MHz, the FWHM of the field of view is 332.1′. The survey region has been observed on a regular hexagonal grid with 112′ between field centers. The 1420 and 408 MHz mosaics used in the present study consist of 11 CGPS fields plus the additional three fields observed at latitudes greater than +5.6° having field centers 135.47°, +5.85°; 134.53°, +7.46°; and 133.60°, +5.85°. The polarization mosaics contain the 14 fields described above plus an additional four CGPS fields, which reveal more of the ambient Galactic medium surrounding the W4 region. H I mosaics consist of the pilot project data (Normandeau et al. 1997) plus three additional CGPS fields.

Since the minimum spacing of the DRAO Synthesis Telescope is 12.86 m, data from single-antenna telescopes are added to regain missing large-scale structure. At 1420 MHz, single-antenna continuum, total-intensity data are obtained from the 100 m Effelsberg Telescope (Reich et al. 1990, 1997) for latitudes up to +4° and from the Stockert 25 m northern sky survey (Reich 1982; Reich & Reich 1986) for higher latitudes. The Effelsberg Telescope has a resolution of 9′, whereas the Stockert Telescope has a resolution of 35′. The Effelsberg data were absolutely calibrated using the Stockert survey data, which ensures consistency among the contributions from the short-spacing data. Short-spacing information is only added to the 1420 MHz total intensity continuum maps (Stokes I) and not to the Stokes Q or Stokes U polarization maps. At 408 MHz, short-spacing data are obtained from the all-sky map of Haslam et al. (1982) with a resolution of 51′. For the spectral line data, short-spacing information was collected using the DRAO 26 m Telescope.

The radio continuum emission at 1420 MHz is observed in four discrete 7.5 MHz bands centered at ±6.25 and ±13.75 MHz from the H I spectral line frequency of 1420.406 MHz. This leaves a 5 MHz gap at the central frequency, which is sufficient to avoid contamination from the H I spectral line. The central 1 MHz of the gap is used for the spectral line observations. The four continuum bands are combined when producing the images used in this paper (Stokes I, Stokes Q, and Stokes U).

Taylor et al. (2003) indicate that there is an uncertainty in the absolute scale of the 408 MHz data of up to ∼15% due to uncertain calibration data. The internal precision of the data is unaffected by this error.

2.2. *Reduction and Processing*

The processing of all CGPS fields and the addition of short-spacing data in all fields were carried out by members of the CGPS data processing team using custom software developed at DRAO (Willis 1999; Taylor et al. 2003). Processing of the additional, high-latitude fields and the mosaicking of the fields were carried out by the authors using the DRAO software, with the assistance of the CGPS data processing team. The higher latitude data were processed, calibrated, and supplemented with short-spacing data such that they matched the CGPS survey data.

3. RESULTS

3.1. *Mosaics*

Mosaics showing the H I spectral line emission at velocities of interest are shown in Figures 1, 2, 3, and 4. The mosaics

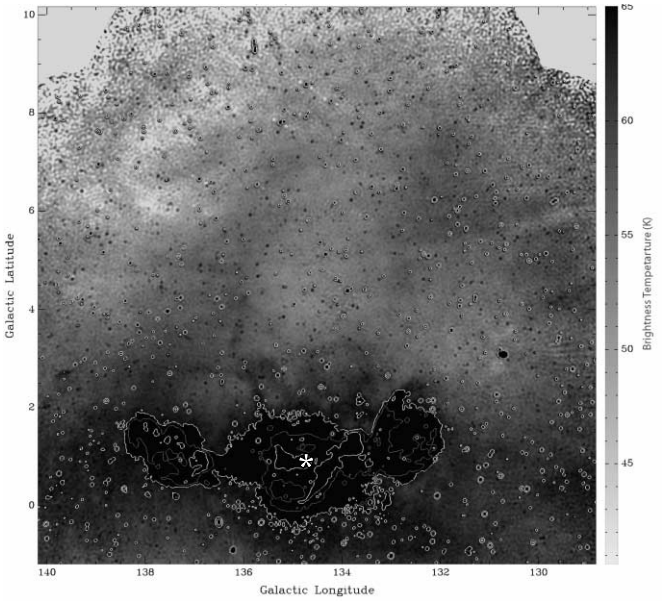

FIG. 5.—Continuum image at 408 MHz (74 cm) linearly scaled to show the faint emission. The resolution is ~3.7′. The white contours are at levels of 120 and 65 K. The gray contour is at 80 K. The latitude and longitude scales shown have units of degrees. The asterisk marks the approximate location of OCl 352.

of continuum emission at 408 and 1420 MHz, Stokes I, Q, and U, are presented in Figures 5, 6, and 7. The grating rings that remain visible in the H I and polarization data are due to the high-intensity sources W3 and 3C 58. The 1420 MHz data were convolved to match the lower resolution (~3.7′) of the 408 MHz data.

The polarization data were convolved to a resolution of 5′ to improve the signal-to-noise ratio, and the Stokes Q and U images were combined to produce a polarized intensity (PI) image [$\mathrm{PI} = (Q^2 + U^2)^{1/2}$] and a polarization angle map [$\psi = \frac{1}{2}\arctan(U/Q)$; see Fig. 8]. Measurements of Stokes I intensities and PI for 56 regions of interest are tabulated in West (2003).

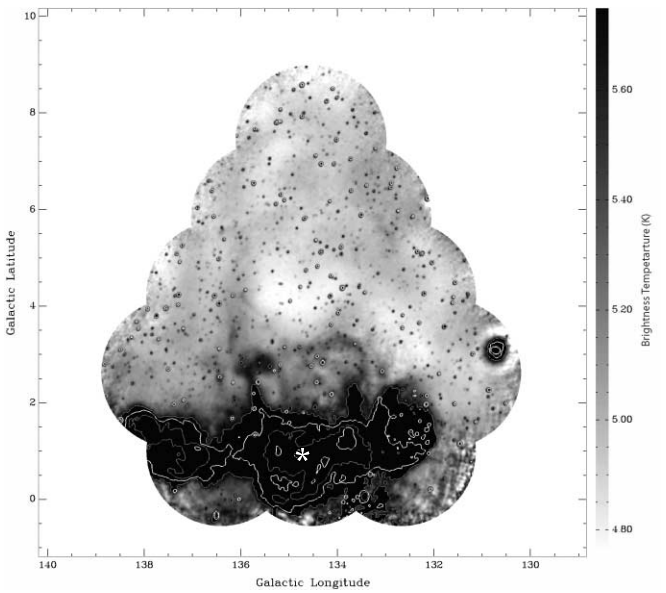

FIG. 6.—Stokes I continuum image at 1420 MHz (21 cm) linearly scaled to show the fainter regions and convolved to match the lower resolution of the 408 MHz data (~3.7′). White contours are set at levels of 16 and 6.5 K, and gray contours are set at 8.5 and 5.75 K. The latitude and longitude scales shown have units of degrees. The asterisk marks the approximate location of OCl 352.

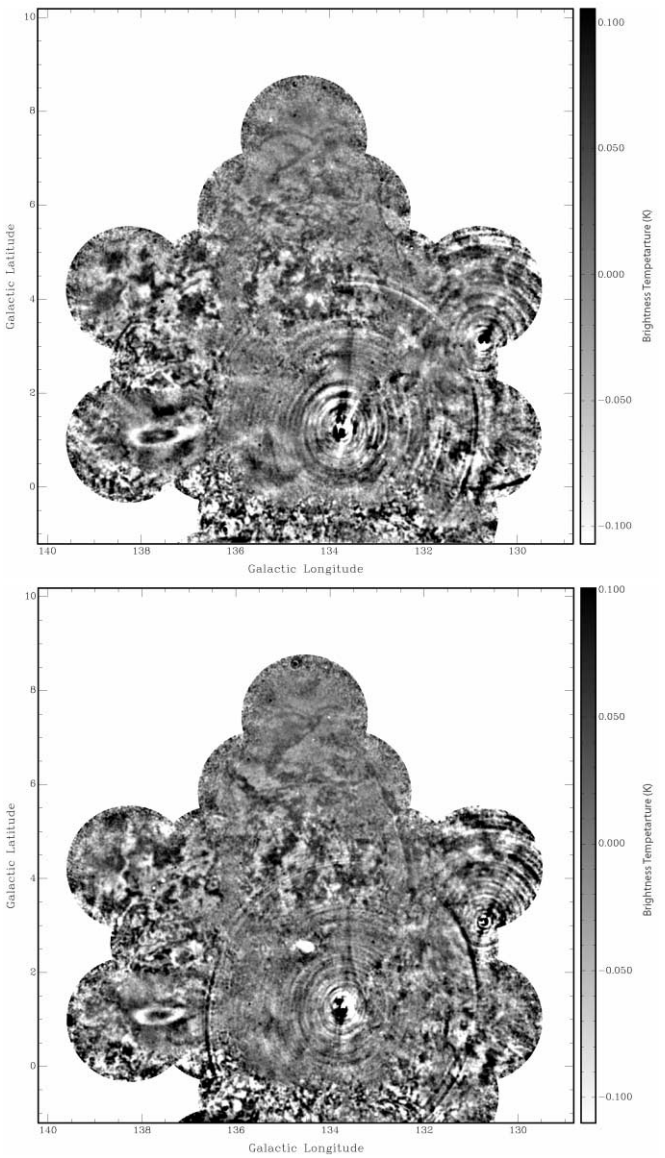

FIG. 7.—Stokes Q (*top*) and Stokes U (*bottom*) images at 1420 MHz (21 cm) convolved to a resolution of 5′. Rings are artifacts due to the bright sources W3 (*center*) and 3C 58 (*right*). The latitude and longitude scales shown have units of degrees.

3.2. H I

3.2.1. *The Atomic Hydrogen Structure of G134.4+3.85*

Figure 1 shows the H I data at $v_{\mathrm{LSR}} = -43.40$ km s^{-1}. The eastern H I wall of the superbubble is clearly visible up to +5.5°, at which point it curves slightly inward and disappears. The western wall is only well defined up to +3.4°. In the new data set presented here, there is no evidence of a cap at high latitudes in the H I data. At lower latitudes, the cavity spans five channels and LSR velocities −38.46 to −45.05 km s^{-1}. We consider the region defined by $133.55 < \ell < 135.5$ and $6° < b < 7°$, the latitudes associated with the Hα shell described by DTS97. We assume that the cap would have a velocity width of five channels (8 km s^{-1}), the velocity width of the cavity. Averaging the signal over five channels, we could have detected a cap of column density 4×10^{19} cm^{-2}. Using five channels reduces σ from the value of the rms noise in a single channel, which is 3.3 K or 1.6×10^{19} cm^{-2}. Thus, if such a cap had been detected its column density would be at the 6 σ level. The observed column

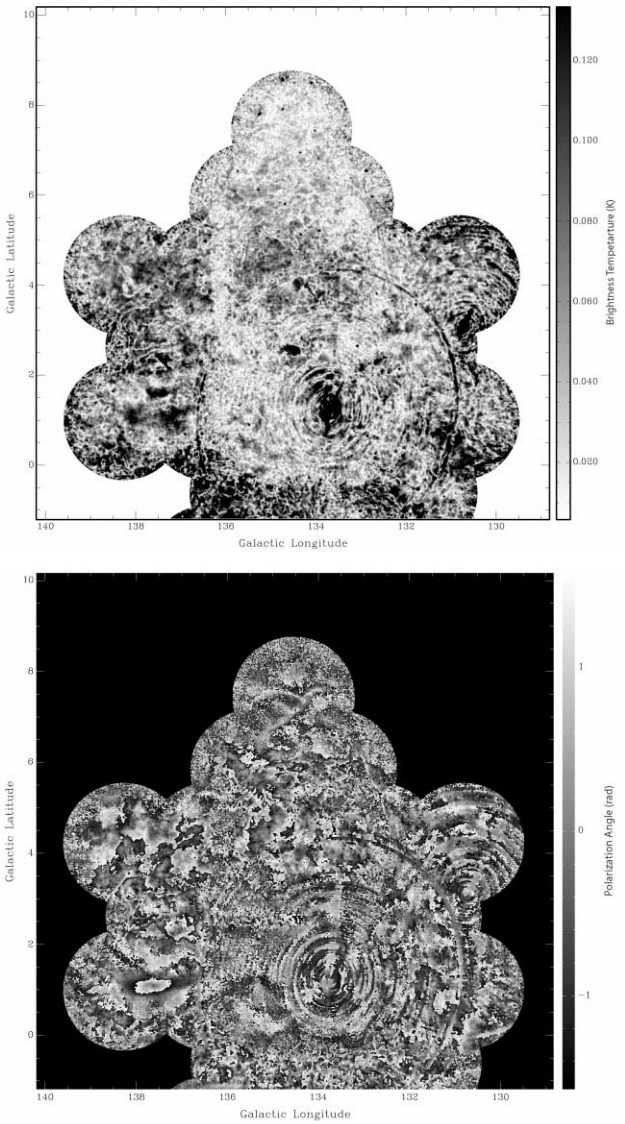

FIG. 8.—Polarized intensity (PI) image (*top*) and polarization angle map (*bottom*) at a resolution of 5′. In the PI image, the gray scale is in kelvins and runs from 0 K (*white*) to 0.140 K (*black*) such that highly polarized regions appear black and depolarized regions show white. Note the depolarization along the walls of the region extending vertically upward at $\ell \approx 136^\circ$ and $\approx 133.5^\circ$ visible as regions of low polarized intensity and as a region having a small cell size, respectively. The "wishbone," with approximate center coordinates ($\ell = 134.9^\circ$, $b = +7.17^\circ$), shows gray in PI and is more prominent in ψ as a region of smoothly varying polarization angle (see § 3.3.1). Note also the bright polarized knot centered at approximately $\ell = 134.5^\circ$, $b = +2.58^\circ$ and showing as black in PI (see § 3.3.2). The interesting lenticularly shaped feature in ψ centered at approximately $\ell = 137.5^\circ$, $b = +1^\circ$ was discussed as likely being caused by a foreground object in Gray et al. (1998, 1999). The latitude and longitude scales shown have units of degrees.

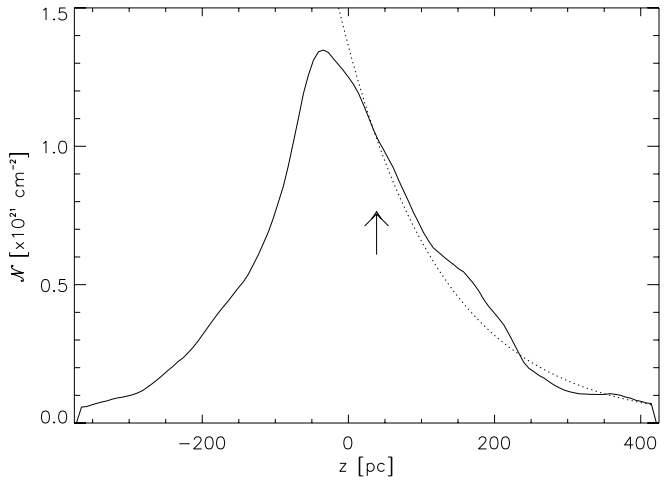

FIG. 9.—H I column density near G134.4+3.85 for the velocity interval -41.76 to -45.05 km s^{-1}. The column density was evaluated from the low spatial resolution 26 m Telescope data, which cover a greater latitude range than the Synthesis Telescope data. The latitude of the cluster OCl 352 is indicated by the arrow. The dotted line is an exponential fit to the decrease in $N_{\rm H}$. The implied scale height is approximately 140 pc. A distance of 2.35 kpc is assumed.

density in the top of the ionized bubble is 1×10^{19} cm^{-2}. By comparison, the column density of electrons in the DTS97 Hα shell is $\sim 1 \times 10^{19}$ cm^{-2}. For this latter estimate we converted emission measure into column density using an average of DTS97's measurements of four points in the upper shell, $T = 10^4$ K, their emission measure conversion of 1 R = 2.8 pc cm^{-6}, and their shell thickness estimate of 10–20 pc. If there was neutral material associated with this Hα shell at a density comparable to that of the ionized material, we would not have been able to detect it.

There is a small filament of H I pointing upward, away from the plane (Fig. 2). This low-level feature is present in four channels of the mosaic, from -41.76 to -46.70 km s^{-1}. A line through this linear feature passes through OCl 352. We argue in § 6.1 that this is material within the superbubble that remains neutral, protected from the ionizing radiation by shadowing. This faint arc is well below the latitude of the cap claimed by DTS97 and therefore below the upper boundary of the best-fit Kompaneets model found by BJM99. Furthermore, the upper tip of the vertical filament is above the ionized cap suggested by the DTS97 data.

It is noticeable that the OCl 352 cluster is at the base of the H I cone, as was described by NTD96, whereas the Kompaneets model by BJM99, which was fit primarily to the Hα image, shows a bubble extending to lower latitudes, to the base of the ionized gas loop that forms the lower half of W4.

This conical shape is not unique—something similar is seen at the base of the Aquila supershell (Maciejewski et al. 1996). The W4 cone extends approximately 200 pc upward from the OCl 352 cluster, based on the well-defined upper longitude wall. This is comparable to the cone at the base of the Aquila supershell, which extends roughly 175 pc for an assumed distance of 3.3 kpc.

3.2.2. *Scale Height in the Vicinity of G134.4+3.85*

The most surprising result from the modeling by BJM99 is the implication of a very small scale height (H), namely, 25 pc. This value was obtained by matching the aspect ratio of the superbubble as seen in Hα using the Kompaneets model and assuming a distance of 2.35 kpc.

Using the data from the 26 m Telescope, which extends farther up in latitude, almost to $+10^\circ$, and fitting an exponential to the decay in column density, a scale height of 140 ± 40 pc is found for the H I in the vicinity of G134.4+3.85 (see Fig. 9). A variety of different velocity intervals were used to test the robustness of this result, as well as different data sets (26 m data, CGPS pilot project data, and CGPS data), and all yield a scale height of approximately 140 pc, which is significantly larger than the 25 pc required by the model of BJM99. Our value compares well with the value of 135 pc quoted by Lockman et al. (1986).

Apart from the contradiction with the prediction by BJM99, this result is not particularly surprising: scale heights for the neutral medium are in the 100–200 pc range. But while the fit

of the Kompaneets model to the shape of the W4 superbubble is very good, it clearly does not address all of the physical processes occurring in this vicinity. In particular, magnetic fields may have contributed to the collimation (Kolmjenovic et al. 1999; de Avillez & Breitschwerdt 2005; see § 6.2).

It should be noted that the scale height evaluated here used data from all longitudes covered by the available 26 m data, from 124.4° to 144.4° with varying coverage in latitude. However, if only longitudes greater than those corresponding to G134.4+3.85 are used, the profile is greatly different for latitudes below +6°, particularly between +1.5° and +4.0°, where the high-longitude data show a plateau instead of a decrease. The difficulty lies in deciding which profile is representative of the medium into which the superbubble expanded. The effect of including G134.4+3.85 itself in the longitude range is minor compared to the effect of what appears to be a partial shell at lower longitudes, which may be associated with 3C 58. These difficulties generate the uncertainty of ±40 pc associated with the 140 pc scale height used in this paper.

3.3. *Polarization*

Gray et al. (1999) presented polarization data from the low latitudes ($b < +4°$) of this region. The high electron density combined with the magnetic field in the W3/W4/W5 region act as a Faraday screen, causing the polarized, background Galactic synchrotron radiation passing through the plasma to be rotated by the process of Faraday rotation. These effects are observationally recognized as depolarized regions that follow the contours of the H II regions. Depolarization occurs when the polarization angle varies by a significant amount between vectors contributing to a single measurement. The polarization angle can differ between adjacent lines of sight sampled by a single telescope beam (beamwidth depolarization) or vary along the path length (depth depolarization). A third depolarization mechanism, bandwidth depolarization, becomes important if the rotation measure (RM) is very high at the observing wavelength, so the angle may change by a large amount across the observing band. Bandwidth depolarization is not significant in this study because for the general ISM, $|\mathrm{RM}| < 300$ rad m^{-2} usually holds and to produce significant depolarization over the 35 MHz observing band of these observations, a RM of ∼1400 rad m^{-2} would be required (Brown 2002).

In Figures 7 and 8 we see that the depolarization extends without interruption from W4 up the walls of G134.4+3.85. This is seen in Stokes *Q* and *U* and in polarized intensity. The continuity of depolarization from W4 to the walls of the superbubble provides strong evidence that the superbubble is connected to the H II region; this is not a chance superposition. A temperature spectral-index map (West 2003) also suggests that W4 and G134.4+3.85 are a single coherent structure.

3.3.1. *The Wishbone*

An unusual wishbone-shaped feature is visible in both Stokes *Q* and Stokes *U*, as well as in polarized intensity and polarization angle maps. This feature has no counterpart in Stokes *I*, total intensity. The feature appears above G134.4+3.85 with approximate center coordinates (134.9°, +7.1667°) (see Figs. 7 and 8). The morphology of the object suggests a shell-like structure. A local steepening of the spectral index is observed south of the wishbone (West 2003).

3.3.2. *Comma-shaped Polarization Feature*

A bright, comma-shaped knot of strong polarized intensity with approximate center coordinates (134.5°, +2.58°) is particularly prominent in polarized intensity (Fig. 8) but invisible in total intensity. It is ∼0.5° wide and ∼0.2° high and has a peak polarized intensity of 0.46 K. The object appears near the base of the prominent V-shaped filaments that are visible in both H I and 60 μm *IRAS* dust emission. However, there is no clear morphological evidence of an association.

The SIMBAD database was searched for catalog objects that might be coincident with the comma-shaped knot on the plane of the sky. A prominent object in this region is an O8 star, BD +62 424, with coordinates (134.53°, +2.46°). There have been two distinctly different heliocentric radial velocity measurements for this star: Abt et al. (1972) measured a value of −42.5 km s^{-1} (−40.2 km s^{-1} LSR), while Fehrenbach et al. (1996) measured a value of −9 km s^{-1} (−6.7 km s^{-1} LSR). The measurement by Abt et al. is consistent with the chimney velocities as observed in the H I spectral line. However, the radial velocity measurement of Fehrenbach et al. (1996) yields a kinematic distance of ∼800 pc (Brand & Blitz 1993) implying that this star is a foreground object. The high polarized intensity of this knot suggests that it may be closer than the W4 region as it suffers less depolarization than does the surrounding region.

4. INTERRELATIONSHIP BETWEEN EMISSION COMPONENTS

To aid in comparison of the various wavelengths, a color image combining the data sets is shown in Figure 10. This image illustrates that there is a correlation between the radio continuum and Hα emission but that the *IRAS* emission seems uncorrelated. The H II regions W3, W4, and W5 and the supernova remnants (SNRs) HB 3 and 3C 58, as well as the spiral galaxy Maffei 2, are readily seen. The Hα superbubble, identified by DTS97, is much more apparent in these combined color images than in the individual images. In Figure 11 we outline an egg-shaped bubble and suggest its three-dimensional structure. A feature that seems to be a continuous branch of emission coming off the main shape of G134.4+3.85 has been labeled the "fork."

The new data presented in this paper show strong evidence of radio continuum emission above OCl 352, associated with the W4 loop below the star cluster and extending up to a latitude of $b \approx +6.7°$. The emission seen at 1420 and 408 MHz generally confirms the Hα data set of DTS97 and reveals G134.4+3.85 to have a striking, continuous egg-shaped structure. In addition, the polarization data reveal a depolarized region consistent with the shell-like structure and indicate that thermally emitting material is depolarizing the background synchrotron emission (see §§ 3.3 and 5). On the east wall we clearly see that the ionized material (whose position is judged from the depolarization feature in Figs. 7 and 8) lies inside the neutral material (position judged from Fig. 1). The relative temperature spectral index is flatter within the region outlined by the depolarized shell, and the value of the index indicates that this emission is thermal (West 2003).

Although the data suggest that G134.4+3.85 has a top (we have already noted in § 3.2 that our observations do not have sufficient sensitivity to show atomic gas connected with the ionized material at the top of the shell), the shape does not have a uniform intensity around the perimeter. There are regions of lower intensity that suggest breaks in the continuous structure. Two main breaks appear in the structure, one near the top and one on the lower longitude side near $b = +4°$. These are seen at both radio frequencies and in Hα with closely coincident positions. The center coordinates and approximate widths for the two breaks are listed in Table 1.

At 1420 MHz and in Hα, there is emission, nicknamed the "fork," that branches off the main structure (Fig. 12). A faint

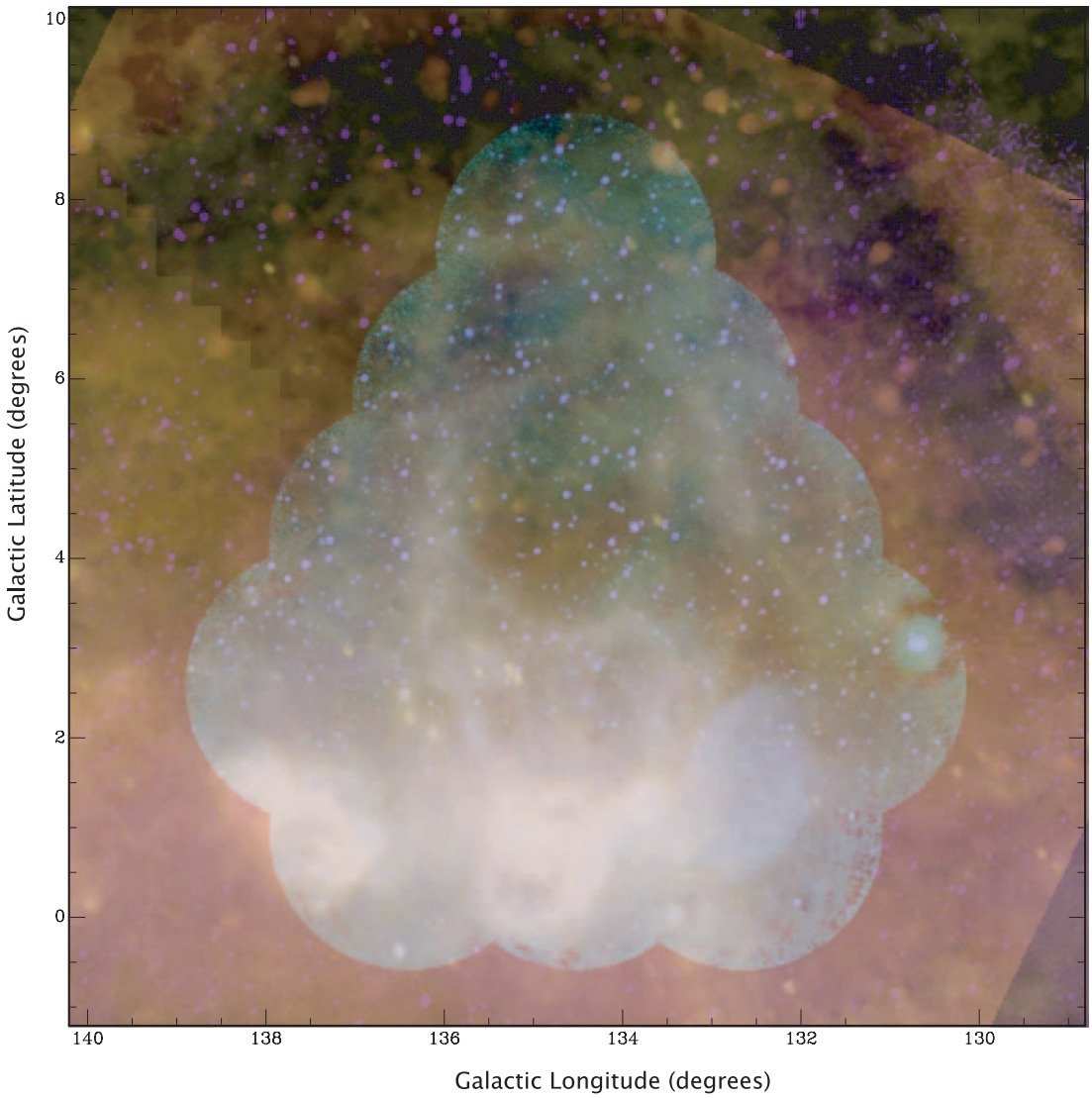

FIG. 10.—Color image combining the data sets: 1420 MHz (*turquoise*), 408 MHz (*purple*), Hα (*red*), and 60 μm *IRAS* (*yellow*). Before combining, the intensities in each set were logarithmically scaled in order to display faint emission. Once colorized, the images were combined. The technique used is analogous to overlaying transparent film images and thus allows details from each data set to be displayed in the final color image. These features are shown here for positional reference. The supernova remnant HB 3 shows a distinct purplish color indicating dominant emission at 1420 and 408 MHz. Regions showing prominently as yellow have high dust emission.

arc of emission extends up from the high-longitude side of the fork and appears to arc westward back to G134.4+3.85. This arc of emission is coincident with the top portion of the polarization wishbone. The lower portion of the fork exhibits depolarization similar to that of the lower portion of the wall, suggesting that the fork is associated with G134.4+3.85. However, it is unclear whether the continuing arc of emission is associated with G134.4+3.85. A hand tracing of the regions of higher emission including the fork and the apparent breaks is presented in Figure 12.

There is a distinctive region of very low continuum emission intensity inside the walls of G134.4+3.85 above $b \approx +3.5^\circ$. It extends up to $+4.8^\circ$ and spans $134^\circ < \ell < 135.5^\circ$. Figure 13 shows plots of the 1420 MHz data at fixed longitude ($\ell = 134.68^\circ$) and fixed latitude ($b = +4.011^\circ$). In both plots this region of very low emission (<4.8 K) is evident; in Figure 13*a* the area runs from $+3.5^\circ < b < +4.8^\circ$ and in Figure 13*b* the area extends from $134^\circ < \ell < 135.5^\circ$. The region has lower emission than in even the regions exterior to G134.4+3.85. This low-emission region is most obvious at 1420 MHz but is also apparent in both 408 MHz and Hα. There appears to be 60 μm emission in this region from dust, which one could reasonably expect to find in the foreground along the line of sight. The low emission implies either that the region is evacuated of plasma that would emit at these wavelengths or that, in the case of the Hα data, UV photons contained within are being absorbed by dust. In the former case, there would be lower plasma column density along the lines of sight passing through this region, producing a lower observed intensity.

In this low-emission region, there are two horizontally oriented H I filaments positioned at $b \approx +3.75^\circ$ that were first identified by NTD96. These are either foreground or background features although, judging by their radial velocity, quite likely to be in the vicinity of G134.4+3.85. They are unlikely to be within it, given the evidence that ionization extends to much higher latitudes.

In addition, a ridge of Hα and 1420 MHz emission appears at $b \approx +3^\circ$ to $+3.5^\circ$. The ridge at 1420 MHz is visible in Figure 6.

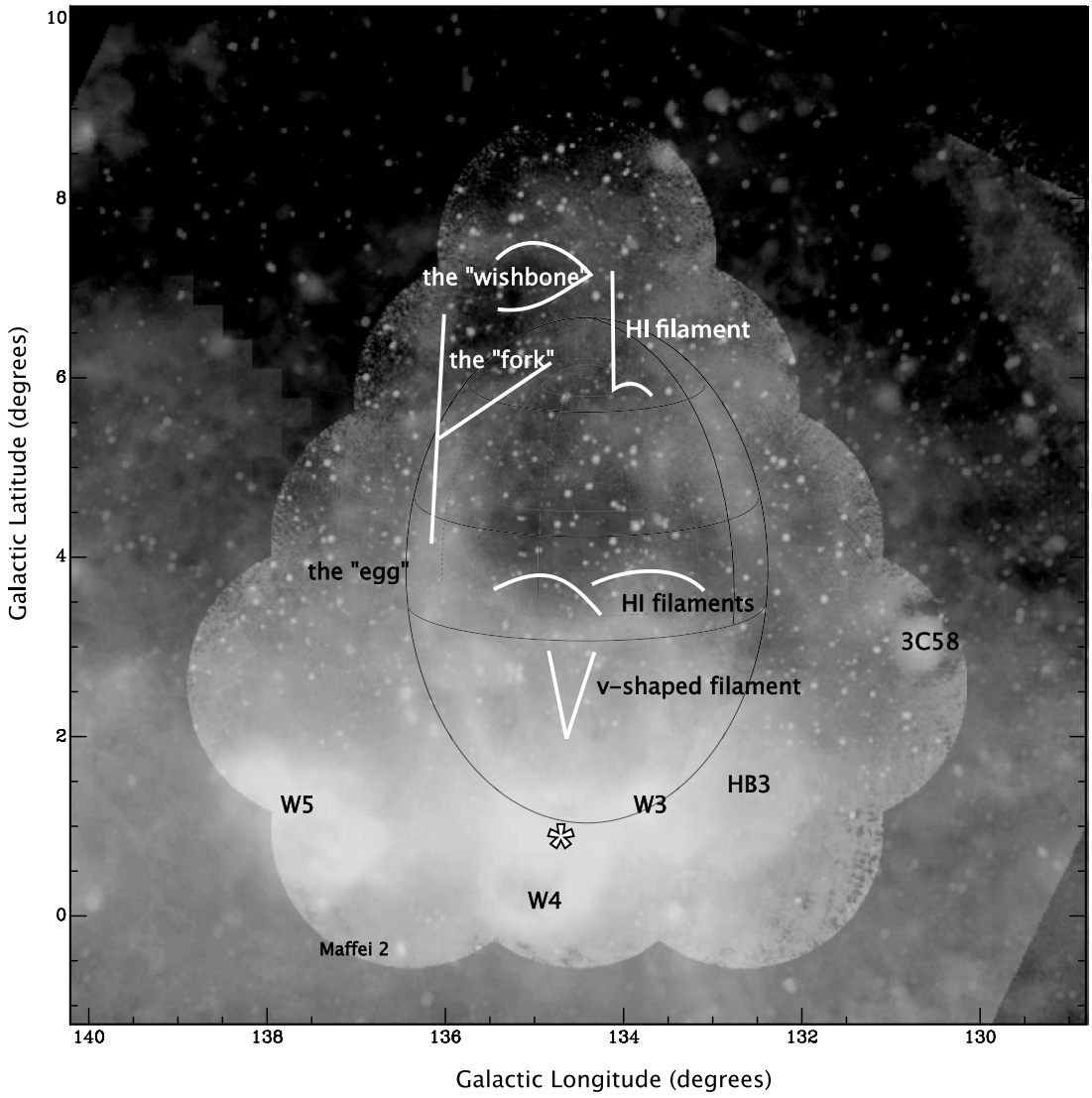

FIG. 11.—Gray-scale version of the image as described in Fig. 10 with labels. The labels identify objects with catalog designations as well as prominent features visible in the data sets. G134.4+3.85 traces the continuous structure apparent in these data. The "wishbone" is a feature visible in the polarization data, and the V-shaped and other filaments are H I spectral line features (NTD96). The asterisk marks the approximate location of OCl 352.

Coincident with the 1420 MHz ridge is a flattening of the temperature spectral index, and below this ridge but above DTS97's point O (West 2003) the spectral index steepens, indicating a shift between these two features (West 2003). This supports the picture of a lower region containing electrons and ionizing radiation (at $b < +3.75^{\circ}$) with an evacuated region above the ridge (at $b > +3.75^{\circ}$).

To summarize, although the structure appears open in the H I images, data showing the ionized gas, along with polarization and temperature spectral index maps, delineate an egg-shaped bubble with a shell that appears to be broken in at least two locations. The temperature spectral index map and Hα data suggest that radiation may possibly be constrained to the lower part of the bubble by a ridge that is evident in Hα and 1420 MHz data.

5. MAGNETIC FIELD ESTIMATE

Rotation measures of extragalactic sources seen through the bubble were measured in an attempt to determine the magnetic field in the shell (West 2003), but the uncertainties are large and the number of sources is small, allowing $B_{\parallel}$ to take any value between 1 and 24 μG. Since rotation measure analysis does not constrain the magnetic field well, we use the following approach

TABLE 1
CENTER COORDINATES AND APPROXIMATE WIDTHS OF BREAKS IN G134.4+3.85

Feature	1420 MHz (deg)	408 MHz (deg)	Hα (deg)	Width[a] (deg)
Upper break	134.77, +5.58	134.12, +5.82	135.08, +5.97	0.5 (20 pc)
Side break	133.47, +4.36	132.84, +3.73	133.56, +4.15	1.2 (49 pc)

[a] The values in parentheses are for an assumed distance of 2.35 kpc.

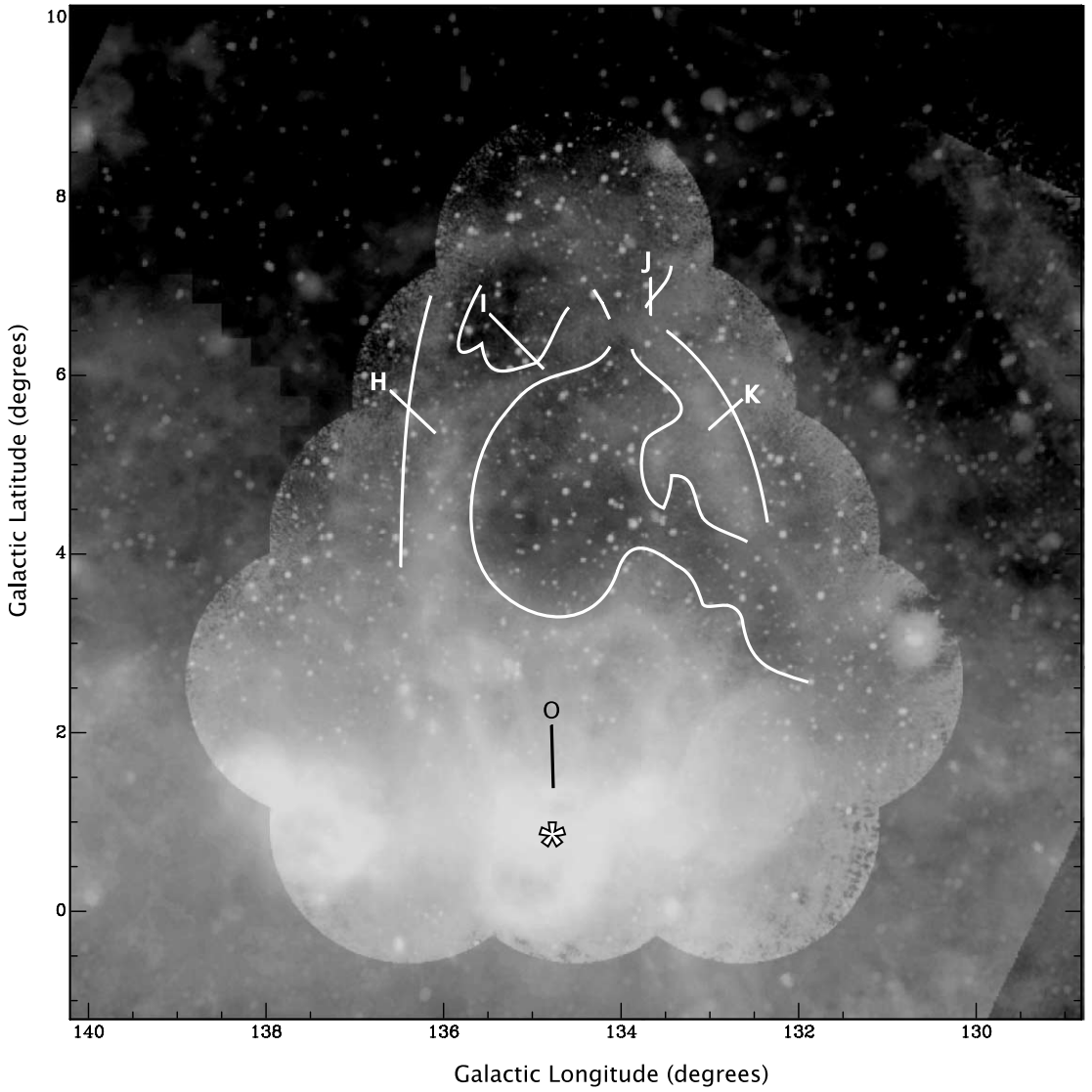

FIG. 12.—G134.4+3.85 and lines tracing the contours of higher emission showing the fork and the two breaks. The data sets are described in Fig. 10. The points labeled alphabetically are regions measured in Hα emission by DTS97. These Hα features are discussed in § 6.1. The asterisk marks the approximate location of OCl 352.

based on depolarization in the walls of the shell. We noted above that the walls of G134.4+3.85 are seen in our data as regions of low polarization relative to the surroundings of the superbubble and that they join smoothly to the depolarization region coinciding with W4 (Gray et al. 1999). From the observed degree of depolarization in the walls we can derive an estimate of the magnetic field in the shell of the superbubble. We use the electron density derived from the Hα measurements of DTS97 and base our calculation on an assumed geometry of the walls.

The electron density is derived from the Hα flux measurements of DTS97 measured at four locations along the upper arc ($b > +5^\circ$) of the shell (DTS97's points labeled H, I, J, and K; see Fig. 12). We estimate the shell thickness, s, from the projected intensity to be between 10 and 20 pc. If we assume a temperature of 10^4 K, use 1 R (Rayleigh) as equivalent to an emission measure of EM = 2.8 pc cm^{-6}, and use DTS97's result that the emission measure of the shell $\sim 5 n_e^2 s$, then n_e is calculated to be 0.44 ± 0.19 cm^{-3} for an assumed shell thickness of 10 pc, or 0.31 ± 0.13 cm^{-3} for an assumed shell thickness of 20 pc. The range of possible electron density is approximately $0.2 < n_e < 0.6$ cm^{-3}.

For the following geometrical argument, we assume that the superbubble is cylindrical, with its axis perpendicular to the Galactic plane (and therefore perpendicular to the line of sight). Its cross section is circular, with outer diameter 80 pc and wall thickness between 10 and 20 pc. The line of sight passes through the cylinder of ionized material in which the electron density is assumed to take the values derived above, and the polarized synchrotron background emission will suffer Faraday rotation on passage through this material if a magnetic field is present and has a line-of-sight component. The path length through the wall of the cylinder for adjacent lines of sight will differ, so the amount of Faraday rotation will differ. If the rotation is sufficiently different for adjacent paths within the telescope beam, there will be significant beam depolarization. The data presented in Figures 7 and 8, where the angular resolution is 5′, indicate that the depolarization amounts to ~50%, implying that the Faraday rotation on lines through the shell separated by 5′ differs by about 60°. At the distance of G134.4+3.85 (2.35 kpc), 5′ corresponds to a physical distance of 3.5 pc. A simple geometrical calculation shows that two paths through the center of the wall of the cylinder, separated by a distance 3.5 pc transverse to the line of

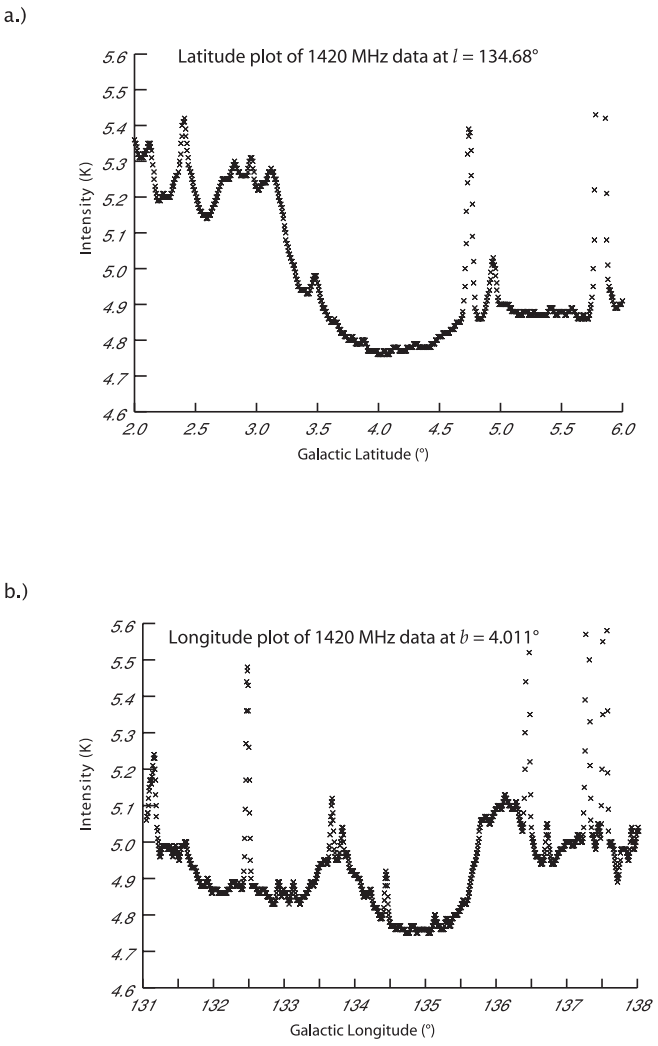

FIG. 13.—(*a*) Plot of intensity vs. Galactic latitude in the 1420 MHz data at a fixed longitude of 134.68°. (*b*) Plot of intensity vs. Galactic longitude in the 1420 MHz data at a fixed latitude of +4.011°.

sight, will differ in length through the wall by $\Delta l = 13$ pc if the wall thickness is 10 pc and by $\Delta l = 19$ pc if the wall thickness is 20 pc.

The Faraday rotation is

$$\Delta\theta = 0.81\lambda^2 n_e B_{\|} \Delta l, \quad (1)$$

where λ is the wavelength, n_e is the electron density, $B_{||}$ is the line-of-sight component of the magnetic field, and Δl is the path length. Inserting the values $\Delta\theta = 60^\circ$ and $\lambda = 0.21$ m, with values for n_e and Δl derived above, we find 3.4 μG $< B_{\|} <$ 9.1 μG. The field derived for the average parameters ($n_e =$ 0.38 cm^{-3} and $\Delta l = 15$ pc) is $B_{\|} = 5.0$ μG.

The range of possible values of electron density in the walls of the superbubble, $0.2 < n_e < 0.6$ cm^{-3}, is 10–30 times the ambient electron density in the vicinity of W4, $\sim$0.02 cm^{-3} (Taylor & Cordes 1993). This implies that the material in the walls of G134.4+3.85 has been compressed by this factor. The value of $B_{\|}$ at this longitude is expected to be $\sim$1 μG, and $B_{\rm total}$ is about 4 μG (Beck 2001). If B varies as $n^{0.5}$, then we expect $B_{\|}$ in the walls of the bubble to be between 3.1 and 5.5 μG, compatible with the above field estimate.

However, we need to consider the likelihood that magnetic field and electron density would be uniform, as is assumed in our field calculation. In the Q, U, and PI images (Figs. 7 and 8) the surroundings of G134.4+3.85 present a mottled appearance that is strongly suggestive of a nonuniform magnetoionic medium. If we think of the medium as divided into cells in which the field and electron density are more or less constant, then the size of the cells appears to be about 20′ in the surroundings. With a compression factor of 10–30, the linear dimension of the cells will shrink by the square root of the compression factor to about 4′. Beam depolarization, which would arise from averaging across many cells, is then unlikely to be significant in the 5′ data, and the geometrical effect we have proposed seems to be an adequate description of the processes leading to the observed depolarization.

Nevertheless, there is still a problem. At 1′, the full resolution of the observations, we would expect to see much less depolarization, both when the geometrical effect is dominant and when the bubble walls contain many cells, and we should not see the bubble walls as significant depolarization features. However, at 1′ resolution the eastern wall of the bubble is still detectable as a depolarization feature (although the western wall is not). There must be some cells in the eastern wall as small as 1′, but we cannot place a precise value on the extent of this small-scale structure because the signal-to-noise ratio at 1′ is very low. The level of polarized intensity in the eastern wall relative to that of the surroundings is very roughly 1.6, although the uncertainty in this ratio is so high that we cannot claim that it is higher or lower than the value of 2.2 ± 0.3 measured from the data at 5′ resolution.

In conclusion we note that BJM99 propose the presence of a swept-up magnetic field, tangential to the shell of the W4 chimney/superbubble, that potentially has a stabilizing effect on the structure (by suppressing Rayleigh-Taylor instabilities that tend to break up the shell). Kolmjenovic et al. (1999) use magnetohydrodynamic modeling to argue that a *vertical* magnetic field of a few microgauss is required to explain a bubble structure that is so highly collimated and to provide the required stabilizing effect. Our depolarization observations indicate that a line-of-sight component of 3–5 μG exists in the shell. However, this measurement does not exclude the possibility of a stronger vertical component, giving a total field of 4–7 μG or larger.

6. DISCUSSION

6.1. *Superbubble or Chimney?*

At our adopted distance of 2.35 kpc, the projected ellipse of G134.4+3.85, which measures $\sim$4° wide by $\sim$6° high, has physical width $\sim$164 pc and height $\sim$246 pc. It has risen to almost twice the scale height of the H I, $\sim$140 pc, determined in § 3.2.2, and at that level the H I density is only 13% of its midplane value (Fig. 9). Nevertheless, the bubble has not reached the halo, considered to begin at a height of $\sim$500 pc (Lockman et al. 1986). Two-dimensional (2D) numerical simulations (e.g., Mac Low et al. 1989) and analytic theoretical explorations (e.g., Ferrara & Tolstoy 2000) indicate that at a distance away from the plane of about 3 scale heights a bubble will accelerate and break out into the halo, creating a chimney. Not only has G134.4+3.85 not reached this height, it may not have the high levels of input wind (or supernova) energy to do so. Most treatments of a single superbubble evolving in a uniform environment indicate that substantially more driving energy is required for breakout. For example, Mac Low et al. (1989) show that a bubble driven by a mechanical luminosity of 1.67×10^{38} ergs s^{-1}, more than 5 times the output of OCl 352, will break out into the halo. Tomisaka (1998) describes the evolution of a bubble driven by 3×10^{37} ergs s^{-1}, equal to the mechanical luminosity of OCl

352, and show that it is unlikely to break out and furthermore is stabilized by the ambient magnetic field.

McClure-Griffiths et al. (2003) describe the Galactic chimney GSH 277+00+36, perhaps a counterexample to G134.4+3.85. This is clearly a chimney, very empty inside, with very complex H I structures in the walls, interpreted as hydrodynamic instabilities. In this case the gas flow within the chimney has had a major impact on the neutral gas forming its walls. We see no such features in G134.4+3.85. Furthermore, GSH 277+00+36 reaches a height of 1 kpc above the Galactic plane, at least 4 times as high as G134.4+3.85. G134.4+3.85 either is driven by a smaller mechanical energy than is GSH 277+00+36 or is at a much earlier stage of evolution.

Thus, the data we have presented seem at first glance to support a picture in which G134.4+3.85 is a superbubble, not a chimney. The structure of ionized gas tapers at the top, suggesting convergence or closure. The 1420 MHz and Hα data clearly show this converging top, and, to a lesser degree, so do the 408 MHz data. There is no cap of neutral material at the upper levels in our H I data. Nor is there any detectable neutral shell surrounding the ionized one; rather, G134.4+3.85 appears as a cavity in the surrounding medium. The H I images do, however, show the diverging conical shape exhibited by chimney models (Norman & Ikeuchi 1989). These observations can be understood in terms of the picture presented by BJM99. In the upper reaches of the bubble the ambient density is dropping rapidly and the ionization structure is unbounded. All neutral gas has been ionized. In this picture, any neutral gas found within the conical void must be protected from UV photons by shadowing. The prime example is the pair of filaments forming a V at $b \approx 2.7^\circ$. A second possible instance, found in our observations, is the vertical H I filament extending from $\sim$(134.15°, +6.083°) to $\sim$(134.175°, +7.25°) and with a width $\sim$0.25° (see Figs. 2 and 11), which appears in several velocity channels from -38.46 to -45.05 km s^{-1}, velocities that are consistent with G134.4+3.85 velocities. These features are linear, or made up of straight-line elements, and are oriented in line with the position of OCl 352.

Although the ionized shell appears closed, our observations have also revealed two gaps; details are given in Table 1. These regions of low emission may well be breaks in the shell. One break is at the top of the bubble, at $b = 6.3^\circ$, and has an apparent width of 20 pc. The ambient density is lowest at the top of the shell, and this is exactly where one might expect the shell to be disrupted. The other break is at lower latitude and appears to be larger, nearly 50 pc wide. In this break we see neither neutral nor ionized material. We interpret these breaks as evidence that the superbubble is fragmenting and turn to an existing theoretical treatment of superbubble breakout and disruption to see what might be learned from it.

We base our discussion on the recent work of de Avillez & Breitschwerdt (2005), who have made high-resolution, three-dimensional (3D) simulations of the magnetized ISM. Their calculations trace in fine detail the evolution of such a medium driven by supernova explosions at the Galactic rate. While they start with a simple, uniform medium, their simulations follow the evolution into the more realistic situation of a medium that becomes highly processed as the result of stellar activity. The morphology of G134.4+3.85 is quite similar to some of the superbubbles shown in their Figure 2. A bubble has developed, centered at $x \approx 0.2$ kpc, $z \approx 0.25$ kpc, in which the higher density skin, rather than forming a closed shell, is open at the top and can be described as filamentary or fragmented. Given its density, this skin can be identified as cool H I gas if the region is in pressure equilibrium. Interior to this skin is a more continuous lower density lining that could be identified with emission from warmer ionized gas. This bubble has protrusions of even hotter gas at both the top and side, which would appear as breaks in ionized gas observations, remarkably similar to the breaks seen in our continuum data for G134.4+3.85. The dimensions of the bubble are approximately 200 pc laterally and 600 pc vertically, somewhat larger than G134.4+3.85

Because of this height, the model bubble can be considered to have reached the Galactic halo at $z \approx 500$ pc. It has been shown with 2D simulations (e.g., Mac Low et al. 1989) that at this altitude of a few scale heights, Rayleigh-Taylor instabilities (in which hot gas pushes into cooler, denser gas) will occur and cause fragmentation of the shell. However, instabilities, Rayleigh-Taylor or other types, can occur at earlier stages, according to the 3D simulations. Indeed the dense skins of smaller bubbles in the de Avillez & Breitschwerdt simulation are also filamentary, indicating that this is so.

Although a magnetic field in the shell can stabilize it against Rayleigh-Taylor instabilities, de Avillez & Breitschwerdt mention that MHD instabilities can occur that will mix the magnetized shell with the ambient medium and cause the escape of hot gas. The field in the skin of their model bubble is a few microgauss or less, and Rayleigh-Taylor instabilities would not be suppressed by this field. The ambient field around G134.4+3.85 is only a few microgauss, but due to compression, the ionized lining of G134.4+3.85 could have a magnetic field strength as high as 7 μG (§ 5). Thus, Rayleigh-Taylor instabilities may be reduced and MHD instabilities, instead, may be the cause of both breaks apparent in G134.4+3.85. The simulations need to be examined in detail in order to assess whether this is the case; M. de Avillez (2006, private communication) has begun such an investigation in relation to G134.4+3.85.

In summary, G134.4+3.85 has now risen into the lower density levels of the Galactic disk but not yet into the halo. Its ionized shell is apparently closed, indicating that it is a superbubble. At high latitudes, the H I distribution retains the conical chimney structure, but that is because the ionized shell is transparent to ionizing radiation. Gaps seen in the shell may well be the first signs of fragmentation of the superbubble and indicate that hot gas is escaping. If so, G134.4+3.85 is on its way to becoming a chimney. The process is likely to accelerate as supernova explosions among the stars of OCl 352 inject energy into the bubble.

6.2. *Timescales and Possible Formation Scenarios*

W4 and its immediate neighbor, W3 (IC 1795), together comprise a complex, highly processed sector of the Galaxy. Many authors have suggested that multiple epochs of star formation have occurred in the region (Lada et al. 1978; Thronson et al. 1980; Carpenter et al. 2000; Reynolds et al. 2001). In particular, Oey et al. (2005) offer evidence that IC 1795 was actually triggered by W4 and that IC 1795 has recently triggered the formation of three ultracompact H II regions around W3. Given that this process is still underway, a question arises: is G134.4+3.85 simply the product of the winds from OCl 352, or has it been shaped by earlier activity? The axis of G134.4+3.85 passes through the position of OCl 352, and there can be little doubt that this star cluster is now driving the evolution of the bubble. However, if winds from earlier massive stars swept out the environment, G134.4+3.85 could have extended to its present height relatively quickly. Oey et al. further argue that the very low scale height ($\sim$25 pc) deduced by BJM99 is the result of earlier clearing

of the environment by a long-gone generation of stars. However, the exact alignment of OCl 352 with the axis of G134.4+3.85 suggests that the superbubble is not simply filling an old cavity, which would most probably have no such alignment.

NTD96 calculate that the combined winds of the nine O-type stars in the cluster could blow out the region up to a height of 110 pc in 5.7 Myr, which roughly agrees with cluster age estimates of 3.7–4.3 Myr. In light of Hα evidence that the structure extends up to $\sim$230 pc, DTS97 calculate that 6.4–9.6 Myr would be required to allow sufficient expansion. They cite cluster ages of 1.3–2.5 Myr, smaller than those obtained by NTD96, and thus claim that OCl 352 cannot be solely responsible for the formation of the Hα superbubble. In passing we note that the calculations of both NTD96 and DTS97 ignored magnetic fields. Ferrière et al. (1991) have shown that a bubble expands more slowly in a magnetized medium: an even longer time would be needed to reach the present size of G134.4+3.85.

Reynolds et al. (2001) observe an Hα loop extending 1300 pc above the midplane of the Galaxy and centered on coordinates (139°, +15°), which they believe is being ionized by OCl 352. They also suggest that multiple star formation epochs have been involved in the formation of this loop and suggest a timescale of 10–20 Myr for the process. If OCl 352 is maintaining the ionization of material 1300 pc above the plane, then the region must be completely clear of neutral material. This is confirmed by our observations, at least to a height of about 300 pc.

We support the suggestion that OCl 352 is the dominant source of ionizing radiation for G134.4+3.85 but that it is not solely responsible for the creation and evolution of the structure. Furthermore, we postulate that there is little matter remaining interior to the upper portion of G134.4+3.85 and that any gas that may have existed at an earlier stage of the life of the superbubble has escaped through the apparent breaks in the structure of G134.4+3.85.

We have presented evidence that there is significant magnetic field in the walls of G134.4+3.85 (§ 5). Ferrière et al. (1991), Tomisaka (1998), and de Avillez & Breitschwerdt (2005) all consider bubbles in the magnetized ISM; all conclude that bubbles elongate in a direction parallel to the field. Tomisaka (1998) concludes that the field will inhibit expansion perpendicular to the field and can also contain the expansion of the bubble. The expansion can still accelerate vertically, even in the presence of a field aligned with the Galactic plane, but only if it is driven by enough energy to reach several scale heights.

What then do we make of the *vertical* elongation of G134.4+3.85? Either it indicates that the scale height is extremely low, as suggested by BJM99, or it implies a field component orthogonal to the Galactic plane (as suggested by Kolmjenovic et al. 1999). Since we do not believe that the scale height is as low as the 25 pc derived by BJM99, we must consider the possibility of a vertical component to the field. Such a component may be the relic of an earlier bubble, and we are compelled by the very shape of G134.4+3.85 to consider that it may have formed in a preprocessed medium, not a pristine one. We can envisage a situation in which a new bubble has filled an old one, and the elongation may have become stronger with each successive wave of star formation. This fits well into the picture of triggered star formation for this complex (Oey et al. 2005) in which the new generation of stars is triggered within the walls of the superbubble created by the preceding generation.

There is also useful insight to be gained from analytical approximations available in the literature. Both Ferrière et al. (1991) and de Avillez & Breitschwerdt (2005) derive analytic equations applicable to a magnetohydrodynamic medium.

De Avillez & Breitschwerdt (2005) calculate the age and the radius (in the equatorial plane) of the bubble when its expansion stalls. Their expression for the age at stall is

$$t_{\max} = 7.2 \times 10^2 L_{37}^{1/2} n_0^{3/4} B_{-6}^{-5/2} \text{ Myr}, \quad (2)$$

where L_{37} is the mechanical luminosity of the stellar wind in units of 10^{37} ergs s^{-1}, n_0 is the density in units of cm^{-3}, and B_{-6} is the ambient magnetic field in units of microgauss. The derivation of this expression is based on the assumption of a uniform ISM and a regular magnetic field. The bubble stalls when the force from thermal pressure is balanced by magnetic force as the bubble distorts field lines. Inspection of equation (2) shows that the stall time is very strongly dependent on the magnetic field but is less influenced by density or driving energy. If the magnetic field goes up by a factor of 4 the time to stall drops by 32!

Nevertheless, the time to stall is long. If we insert $L_{37} = 3$, $n_0 = 0.3$, and $B_{-6} = 2$ (note that this is the ambient field, not the compressed field, and that we use the regular component of the field, ignoring the random component), then we obtain $t_{\max} = 89$ Myr, far longer than the age of OCl 352. If the field is as high as $B_{-6} \approx 5$, this time drops to about 9 Myr, a more reasonable value. The radius of the bubble at stall is

$$R_{\max} = 2.2 \times 10^3 L_{37}^{1/2} n_0^{1/4} B_{-6}^{-3/2} \text{ pc}. \quad (3)$$

For the situation considered above the stall radius is $\sim$1000 pc (for $B_{-6} = 2$) and $\sim$250 pc (for $B_{-6} = 5$). G134.4+3.85 is nowhere near this size, and has not stalled.

However, bubbles do in time stall. Contraction follows stall and occurs mostly in the equatorial region, so old bubbles become quite elongated in the direction of the field (de Avillez & Breitschwerdt 2005). However, we have just demonstrated that G134.4+3.85 has not stalled, so the elongation cannot be the product of contraction but must be the product of an ambient field that already has a strong vertical component. We therefore propose a model in which G134.4+3.85 is driven more by preexisting magnetic field structure than by preexisting density structure; this is consistent with the ideas expressed by de Avillez & Breitschwerdt (2005).

Ferrière et al. (1991) describe a substantial thickening of the wall of a bubble formed in a magnetized medium. In their calculation for $L_{37} = 3.2$, $n_0 = 0.32$, and $B_{-6} = 3$, plausible values for G134.4+3.85, the equatorial shell thickness is about 20% of the radius. From our observations the value of $\Delta R/R$ is between 12% and 24%, quite compatible with their model.

We pursue this idea further and suggest another possible explanation for the observed gaps in the shell. In the analytical models, the shell thickness depends on the location on the shell. The above estimate refers to the magnetic equator; at the magnetic poles the shell becomes very thin. We speculate that this effect might be related to the apparent break in the top of the shell. It is conceivable that it is not a break at all but simply a thin spot. We note that it is exactly at such a thin spot at the magnetic pole that one would expect such a shell to break.

In addition to these magnetic field arguments, we find morphological evidence that supports a scenario with multiple star-forming epochs. Near the cluster there is relatively intense $\sim$22 K emission at 1420 MHz. Around the cluster, but not symmetrically centered on it, is the W4 loop, a 1° ($\sim$40 pc) loop visible in radio continuum, infrared, and Hα emission with shell-like structure. This loop does not have a constant limb brightness and is interpreted as having broken out in places (Terebey et al. 2003).

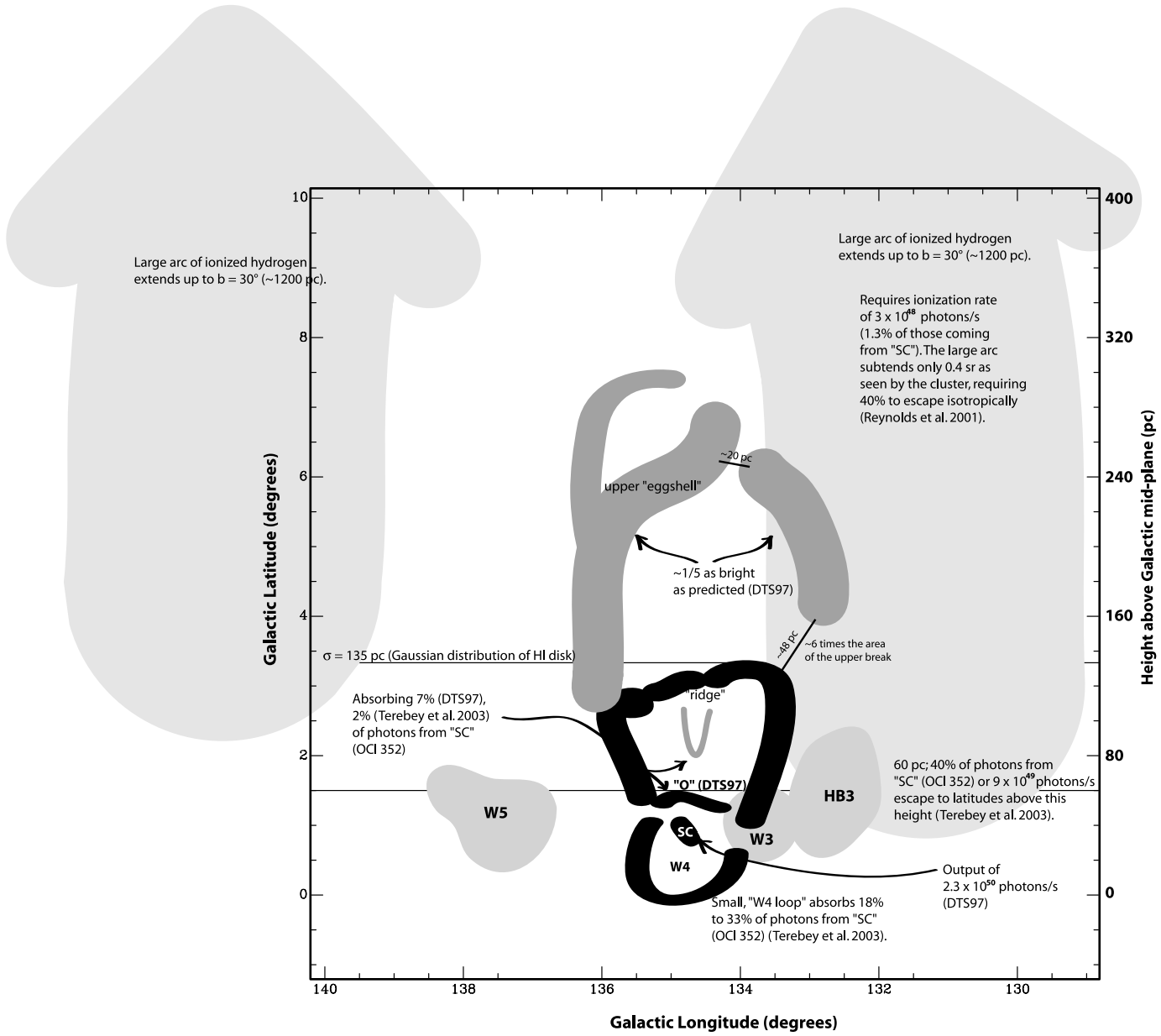

FIG. 14.—Schematic diagram summarizing the results of DTS97, Terebey et al. (2003), and Reynolds et al. (2001) regarding the number of ionizing photons that can escape into the Galactic halo. DTS97 predict that the upper shell should have an intensity of 20 R but it was observed to have $\sim\frac{1}{5}$ this intensity. The region dubbed G134.4+3.85 includes the filaments above $b = +1^\circ$ and extending up to $b = +6^\circ$. This is defined by the egg-shaped structure outlined in Fig. 11. The dark and light gray lines schematically represent the varying intensity of the emission.

Above $b + 1.29^\circ$, the 1420 MHz intensity drops from 8.8 to $\leq$6 K. Between $b \approx +1.5^\circ$ and $\approx$+3.2°, the intensity decreases only slightly, from $\sim$6 to $\sim$5.2 K, after which one finds an arc above which the intensity drops quickly to $\sim$4.75 K in the low-emission region (see Fig. 13). Farther above this we find the upper limb of G134.4+3.85. We postulate that this pattern is the result of a series of star-forming epochs in the region. Detailed theoretical modeling is beyond the scope of this paper but is needed to test whether this postulate is physically reasonable.

6.3. *The Halo Connection*

DTS97 state that the O-type stars in OCl 352 have a total output of $\sim 2.3 \times 10^{50}$ photons s^{-1}. Terebey et al. (2003) conclude that 40% $\pm$ 16% ($\sim 9.2 \times 10^{49}$ photons s^{-1}) of this ionizing radiation escapes to heights above 60 pc. They suggest that these photons are available to ionize the diffuse gas and the upper Galactic halo. Our observations suggest that some of these photons are ionizing the gas in the upper portion of the shell.

DTS97 predict that the Hα surface brightness of the upper portion of the shell should be $\sim$20 R, which is well in excess of the 0.7–6.7 R that is observed. They propose that two small molecular clouds located a little above the W4 loop are shadowing the upper portion of the shell, accounting for the low observed values of the emission measure. In contrast, Terebey et al. (2003) find that fewer photons than predicted by DTS97 are absorbed by the molecular clouds. A schematic diagram summarizing this picture is provided in Figure 14.

We adopt the Terebey et al. picture that 40% of the ionizing photons emitted by OCl 352 are not absorbed by the W4 loop. In light of the H I and continuum data presented here, which are reminiscent of the ionization modeling by BJM99, we propose that some of these photons are ionizing G134.4+3.85, while

others escape through the breaks in G134.4+3.85's walls, and yet others simply pass through the thin, fully ionized upper portion of the shell.

The average value of the observed Hα surface brightness for the four points H–K (see Fig. 12) is 4 R. If we compare this to the predicted 20 R (DTS97) we find that $\sim$20% ($\sim 1.8 \times 10^{49}$ photons s^{-1}) of the photons escaping from the lower loop ionize G134.4+3.85 and the remaining $\sim$80% ($\sim 7.2 \times 10^{49}$ photons s^{-1}) escape.

In summary, the cluster produces of total flux of $\sim 2.3 \times 10^{50}$ photons s^{-1}, of which 40% ($\sim 9.2 \times 10^{49}$ photons s^{-1}) escape the W4 loop according to Terebey et al. (2003). Of the photons escaping the W4 loop, $\sim$20% ($\sim 1.8 \times 10^{49}$ photons s^{-1}) are needed to produce the observed ionization in the upper shell of G134.4+3.85; this is 8% of the total flux. The amount of this ionizing flux is less than the uncertainty in the estimate of the number of photons escaping from the loop. This helps emphasize that the majority of these loop-escaping photons may leave G134.4+3.85 through the breaks and through the thin, fully ionized upper shell.

Reynolds et al. (2001) estimate that the total hydrogen ionization rate for the large Hα loop observed in the WHAM (Wisconsin Hα Mapper) data is 3×10^{48} photons s^{-1}, or $\sim$1.3% of OCl 352's total output. However, given that the loop subtends $\sim$0.4 sr as seen from the cluster, approximately 40% of the cluster's luminosity ($\sim 9.2 \times 10^{49}$ photons s^{-1}) must escape if such escape is isotropic. This is reasonably consistent with our estimate, and we conclude that $(8 \pm 1) \times 10^{49}$ photons s^{-1} escape into the halo.

7. CONCLUSIONS

Compelling evidence has been presented for the existence of a fragmented superbubble that is in the process of evolving into a chimney. Based on low-latitude H I data, the structure, named here G134.4+3.85, was originally postulated to be a fully formed chimney. Later, Hα data suggested that it was closed near $b = +7^\circ$. The radio continuum data presented in this paper show a structure similar to that seen in Hα, although two breaks, one at the top and one in the low-longitude wall, are apparent in the combined data. Polarized intensity images, showing depolarization extending from the W4 H II region up the walls of the superbubble, confirm that the observed continuum emission and Hα emission are at the same distance as the W4 region. In contrast, the H I data make it clear that there is no corresponding neutral shell. We speculate that one of the breaks could be associated with the thinning of the ionized shell at a magnetic pole. However, the two breaks in the ionized skin of the bubble and the lack of a closed neutral H I shell are similar to features in computational simulations (in the literature) of superbubbles that are evolving into chimneys. In these simulations fragmentation can be caused when magnetohydrodynamic instabilities mix the magnetized shell with the ambient medium.

The fraction of ionizing photons emitted by OCl 352 that are not absorbed by the W4 loop is more than sufficient to account for the continuum emission from G134.4+3.85. The excess can escape both through the two breaks observed in the shell and through the thin, fully ionized upper portion of the shell.

G134.4+3.85 is $\sim$165 pc wide and extends $\sim$240 pc above the midplane of the Galaxy, reaching beyond 135 pc, which is the 1 σ height of the global Gaussian H I distribution. While this is not into the Galactic halo, the photons from OCl 352 can contribute to the ionization of the Reynolds layer of the Galaxy and are likely the main source of ionization of the large Hα loop seen in the WHAM data.

The authors would like to thank R. Kothes for assistance with the data processing and A. Gray and J. C. Brown for many helpful discussions.

This work was supported by the National Science and Engineering Research Council of Canada. The Dominion Radio Astrophysical Observatory Synthesis Telescope is a national facility operated by the National Research Council of Canada. The Canadian Galactic Plane Survey is a Canadian project with international partners and is supported by a grant from the Natural Sciences and Engineering Research Council of Canada. Data from the Canadian Galactic Plane Survey are publicly available through the facilities of the Canadian Astronomy Data Centre (http://cadc.hia.nrc.ca). The SIMBAD database is operated at the Centre de Données astronomiques de Strasbourg (CDS), Strasbourg, France.

REFERENCES

Abt, H. A., Levy, S. G., & Gandet, T. L. 1972, AJ, 77, 138
Basu, S., Johnstone, D., & Martin, P. G. 1999, ApJ, 516, 843 (BJM99)
Beck, R. 2001, Space Sci. Rev., 99, 243
Brand, J., & Blitz, L. 1993, A&A, 275, 67
Brown, J.-A. C. 2002, Ph.D. thesis, Univ. Calgary
Carpenter, J. M., Heyer, M., & Snell, R. L. 2000, ApJS, 130, 381
de Avillez, M. A., & Berry, D. L. 2001, MNRAS, 328, 708
de Avillez, M. A., & Breitschwerdt, D. 2005, A&A, 436, 585
Dennison, B., Topasna, G. A., & Simonetti, J. H. 1997, ApJ, 474, L31 (DTS97)
Fehrenbach, C., Duflot, M., Genty, V., & Amieux, G. 1996, Bull. Cent. Donnees Stellaires, 48, 11
Ferrara, A., & Tolstoy, E. 2000, MNRAS, 313, 291
Ferrière, K. M., Mac Low, M.-M., & Zweibel, E. G. 1991, ApJ, 375, 239
Gray, A. D., Landecker, T. L., Dewdney, P. E., & Taylor, A. R. 1998, Nature, 393, 660
Gray, A. D., Landecker, T. L., Dewdney, P. E., Willis, A. G., & Normandeau, M. 1999, ApJ, 514, 221
Haslam, C. G. T., Salter, C. J., Stoffel, H., & Wilson, W. E. 1982, A&AS, 47, 1
Kolmjenovic, P. T., Basu, S., & Johnstone, D. 1999, in ASP Conf. Ser. 168, New Perspectives on the Interstellar Medium, ed. A. R. Taylor, T. L. Landecker, & G. Joncas (San Francisco: ASP), 299
Lada, C. J., Elmegreen, B. G., Cong, H.-I., & Thaddeus, P. 1978, ApJ, 226, L39
Landecker, T. L., et al. 2000, A&AS, 145, 509
Lockman, F. J., Hobbs, L. M., & Shull, J. M. 1986, ApJ, 301, 380
Maciejewski, W., Murphy, E. M., Lockman, F. J., & Savage, B. D. 1996, ApJ, 469, 238
Mac Low, M.-M., McCray, R., & Norman, M. L. 1989, ApJ, 337, 141
McClure-Griffiths, N. M., Dickey, J. M., Gaensler, B. M., & Green, A. J. 2003, ApJ, 594, 833
Norman, C. A., & Ikeuchi, S. 1989, ApJ, 345, 372
Normandeau, M., Taylor, A. R., & Dewdney, P. E. 1996, Nature, 380, 687 (NTD96)
———. 1997, ApJS, 108, 279
Oey, M. S., Watson, A. M., Kern, K., & Walth, G. L. 2005, AJ, 129, 393
Reich, P., & Reich, W. 1986, A&AS, 63, 205
Reich, P., Reich, W., & Fürst, E. 1997, A&AS, 126, 413
Reich, W. 1982, A&AS, 48, 219
Reich, W., Reich, P., & Fürst, E. 1990, A&AS, 83, 539
Reynolds, R. J., Sterling, N. C., & Haffner, L. M. 2001, ApJ, 558, L101
Taylor, A. R., et al. 2003, AJ, 125, 3145
Taylor, J. H., & Cordes, J. M. 1993, ApJ, 411, 674
Tenorio-Tagle, G., & Bodenheimer, P. 1988, ARA&A, 26, 145
Terebey, S., Fich, M., Taylor, A. R., Cao, Y., & Hancock, T. 2003, ApJ, 590, 906
Thronson, H. A., Campbell, M. F., & Hoffmann, W. F. 1980, ApJ, 239, 533
Tomisaka, K. 1998, MNRAS, 298, 797
West, J. L. 2003, Master's thesis, Univ. Manitoba
Willis, A. G. 1999, A&AS, 136, 603